

Density Estimation from Aggregated Data with Integrated Auxiliary Information: Estimating Population Densities with Geospatial Data

Michael Mühlbauer  ¹ and Timo Schmid  ^{*1}

¹Institute of Statistics, University of Bamberg, Bamberg, Germany

Version: Preprint 1.0 (05.08.2025)

Abstract

Density estimation for geospatial data ideally relies on precise geocoordinates, typically defined by longitude and latitude. However, such detailed information is often unavailable due to confidentiality constraints. As a result, analysts frequently work with spatially aggregated data, commonly visualized through choropleth maps. Approaches that reverse the aggregation process using measurement error models in the context of kernel density estimation have been proposed in the literature. From a methodological perspective, we extend this line of work by incorporating auxiliary information to improve the precision of density estimates derived from aggregated data. Our approach employs a correlation-based weighting scheme to combine the auxiliary density with the estimate obtained from aggregated data. We evaluate the method through a series of model-based simulation scenarios reflecting varying conditions of auxiliary data quality. From an applied perspective, we demonstrate the utility of our method in two real-world case studies: (1) estimating population densities from the 2022 German Census in Bavaria, using satellite imagery of nighttime light emissions as auxiliary data; and (2) analyzing brown hare hunting bag data in the German state of Lower Saxony. Overall, our results show that integrating auxiliary information into the estimation process leads to more precise density estimates.

Keywords: Choropleth maps, Geo-referenced data, Kernel density estimation, Regional aggregates

^{*}timo.schmid@uni-bamberg.de

1 Introduction

Understanding the spatial distribution of phenomena is relevant across various fields such as public health (see e.g., Yang et al. (2022), who explore clusters of gastrointestinal tumors), urban planning (see e.g., Brandão et al. (2018) who estimate the distribution of building renovations in Lisbon) and environmental monitoring, where Lin et al. (2010) provides an example of identifying soil pollution hotspots in the Changhua county of central Taiwan. A widely applied non-parametric method for estimating spatial distributions is kernel density estimation (KDE) (see Silverman (2018) for a general introduction and Rosenblatt (1956) and Parzen (1962) for the foundational work on the method), which traditionally requires precise data points, such as exact 2D geocoordinates comprised of longitude and latitude values for bivariate spatial analysis. Such precise data is not always available to analysts due to reasons such as the data collection method or post hoc spatial aggregation implemented to address confidentiality concerns. For example, vaccination data for common diseases such as Tick-borne encephalitis (TBE) and influenza are only published at the level of the German Nomenclature of units for territorial statistics (NUTS)-3 (Rieck et al., 2020). Similarly, the European brown hare (colloquially also referred to as "jackrabbits") hunting bag data used in this paper is also only recorded at the NUTS-3 district level. The Groß–Rendtel–Schmid–Schmon–Tzavidis (GRSST) estimator (Groß, 2016), which is detailed in the next section, is an approach designed for data scenarios characterized by these limitations. The GRSST estimator builds upon the core idea of iteratively enriching a flat pilot KDE estimate with aggregated information, described in Groß, 2016 and extends it to the bivariate context of spatial data. Subsequent literature includes (Groß et al., 2020), which demonstrates how the GRSST can be used to transform area aggregates between non-hierarchical area systems. In Rendtel and Ruhanen (2018), the algorithm is applied in the context of open data to improve the estimation of local childcare needs in Berlin. Later, Rendtel et al. (2021) utilize the concept to enhance the visualization of COVID-19 incidence clusters.

An inherent characteristic of the GRSST estimator, already identified in the original work by Groß (2016), is its dependence on the geographical size of the input data areas. Large areas tend to produce largely homogeneous density plateaus on the insides away from their borders, as there is no input information to support a more accurate estimate within those areas, apart from the aggregated information. This implies that, *ceteris paribus*, the quality of the estimate decreases with fewer and larger input areas. Depending on the context and the underlying distribution, the coarseness of the input areas might be negligible, but when looking e.g. at the NUTS-3 district level and the distribution of the human population, accepting a

lack of information on the distribution inside of the districts intuitively comes with density estimates of decreased quality. Motivated by the spirit of small area estimation (SAE) (see Rao and Molina (2015) for a comprehensive overview), we try to address this shortcoming through the use of auxiliary data. Because oftentimes, analysts may find themselves with auxiliary data that carries some informational value regarding the actual density of interest. For instance, population density tends to correlate with satellite imagery of nighttime light emissions (Sutton et al., 2001). Similarly, in the context of ecological data where the distribution of a certain animal species is only recorded per large habitat area, detailed vegetation maps could provide valuable auxiliary information about potentially preferred microhabitats within those broader zones.

At this point the natural question arises on how to exploit such auxiliary information in order to improve GRSST estimate. To achieve this, we propose an additional step to the GRSST algorithm: forming a convex combination of an auxiliary density, derived from auxiliary data, and the standard GRSST density estimate. The weighting for this combination is based on the correlation calculated between the auxiliary density, aggregated to the spatial level of the GRSST input data, and the GRSST input data itself. We refer to this augmented approach as augmented GRSST (AGRSST). A special case of the AGRSST arises when the auxiliary density is weighted with 1; we shall call this special case AGRSST1. This version essentially relies fully on the auxiliary density and benchmarks it against the GRSST input data. In this paper, we first recall the GRSST algorithm and then introduce our extension, AGRSST. Subsequently, we investigate the performance of the GRSST, AGRSST, and AGRSST1 in a model-based simulation study and later in an evaluation study based on real-world German population data from the 2022 Census. We also apply the AGRSST to brown hare hunting bag data in the German state of Lower Saxony, using remote sensing normalized difference vegetation index (NDVI) data to construct an auxiliary density. Our results indicate that the AGRSST can be a valuable addition to the exclusive use of the GRSST; however, its strong reliance, especially in the AGRSST1 case, necessitates a sound theoretical justification for the auxiliary density. The structure of the paper is as follows: In Section 2, we revisit the GRSST and propose the additional AGRSST step. In Section 3, we evaluate our method in a simulation study. Section 4 presents an evaluation study that applies the AGRSST in the context of population density estimation. In Section 5, we apply our method to a real-world scenario, estimating the density of the brown hare hunting bag. Finally, in Section 6, we conclude our paper with a discussion and final remarks, pointing towards possible future research directions.

2 Methodology

2.1 The Groß–Rendtel–Schmid–Schmon–Tzavidis Estimator

The GRSST estimator was first introduced in Groß (2016) to estimate bivariate densities based on rounded geocoordinate data of ethnic minorities and aged people in Berlin. The estimator is based on a measurement error model which allows the derivation of an iterative procedure reminiscent of the stochastic EM (SEM) algorithm (Celeux et al., 1996) combined with KDE in each iteration. In their original work, Groß (2016) propose the GRSST estimator to address the case of rounded geocoordinates, where precise geocoordinates are rounded to the center points of the rectangles in which they fall. The following formulation of the GRSST estimator is slightly more general, describing the rounding process as the association of a geocoordinate with an area. It is important to note that this formulation is not novel but rather a slight variation of the framework already laid out in Groß et al. (2020). The GRSST algorithm is implemented in the R package `Kernelheaping` (Groß and Fuchs (2022), see Gril et al. (2025) for a detailed tutorial).

We assume a geographical map as the sample space $\Omega = \{(\ell^o, \ell^a) \in \mathbb{R}^2\}$ for the random variable Z of the latent (unobserved) geocoordinates $z_i = (\ell_i^o, \ell_i^a)$, where ℓ_i^o and ℓ_i^a are geographical longitude and latitude values and the index $i \in \{1, 2, \dots, n\}$ refers to the geocoordinates that constitute the total sample size n . We employ $\ell = (\ell^o, \ell^a)$, to denote a geocoordinate location independently of the underlying random variable. Further, Z is assumed to follow a continuous probability density function (PDF)

$$Z \stackrel{iid}{\sim} P_Z(\ell). \quad (2.1)$$

Many applications of the GRSST estimator assume that the entire population is sampled, so $n = N$. We also postulate a random variable $X(Z)$, which maps Z to a set of disjoint sets of geocoordinates, so that $X = f(Z) : \Omega \rightarrow \{A_1, \dots, A_d, \dots, A_D\}$, where $\Omega = \bigcup_{d=1}^D A_d$. Here, A_d denotes the set of all possible geocoordinates that fall inside of the d -th geographical area, and x represents a particular outcome of the random variable X , where this outcome is one of the defined geographical areas A_d . For example, if Ω represents the map of Germany and the D geographical areas are the German NUTS-1 regions, then, since the NUTS-1 level consists of the 16 federal states, $D = 16$. In this case, one specific A_d would be the set containing all geocoordinates within the state of Bavaria. Consequently, the random variable X , representing the observed geographical area, follows a multinomial probability mass function (PMF) with one trial and D categories.

$$X \stackrel{iid}{\sim} P_X(\ell) = \mathcal{M}_{D,1}(\ell), \quad (2.2)$$

which can be evaluated at the geocoordinate level using the map $f(Z)$. The conditional probability distribution of the area X , given a specific latent geocoordinate Z located at ℓ and denoted as $P_{X|Z}(\ell)$, follows a Dirac distribution:

$$P_{X|Z}(\ell) = \begin{cases} 1 & \text{if } \ell \in A_d, \text{ with } x = A_d \\ 0 & \text{otherwise.} \end{cases} \quad (2.3)$$

We can combine these three expressions in Bayes' theorem and obtain

$$P_{Z|X}(\ell) = \frac{P_{X|Z}(\ell) P_Z(\ell)}{P_X(\ell)}. \quad (2.4)$$

This is a measurement error model for the density of the exact, unknown geocoordinate z_i , given the observed area x_i in which it is located. We draw attention to the fact that $P_{X|Z}(\ell) = \mathbb{1}_{\ell \in A_d}(\ell)$, which allows us to rewrite eq. (2.4) as

$$P_{Z|X}(\ell) \propto P_{X|Z}(\ell) P_Z(\ell) = \mathbb{1}_{\ell \in A_d}(\ell) P_Z(\ell). \quad (2.5)$$

Here, we can see that the introduction of x_i via Bayes' theorem essentially limits the possible draws of a geocoordinate z_i to the area A_i in which it is known to be located.

The core idea of the GRSST estimator (formally outlined in Algorithm 1) is to begin with a pilot estimate $P_Z^{(0)}(\ell)$, incorporate the information contained in x_i by sampling according to eq. (2.4) for all x_i , to update to a new $P_Z^{(l)}(\ell)$ (the "E-step"), and minimize the root mean integrated squared error (RMISE) using KDE (the "M-step"). This process is repeated until convergence. Note that the superscript (l) denotes the iteration number, which runs from 0 to $M = L + B$, where B is the number of burn-in iterations and L the number of additional iterations. This algorithm closely resembles the classic expectation-maximization (EM) algorithm (Dempster et al., 1977); however, it is important to emphasize several key differences, which we discuss below.

Algorithm 1 Groß–Rendtel–Schmid–Schmon–Tzavidis Estimator

- 1: Start with a pilot estimate of $P_Z(\ell)$, $\hat{P}_Z^{(0)}(\ell)$ by estimating a KDE with a large bandwidth \mathbf{H} .
- 2: Evaluate $\hat{P}_Z^{(l-1)}(\ell)$ from the last iteration on a fine grid $\mathbf{G} \subset \Omega$ of geocoordinates (grid points) denoted g_j , with index $j \in \{1, 2, \dots, J\}$.
- 3: S-Step: For all i sample from \mathbf{G} using the corresponding value of $P_{X|Z}(x_i|\ell) \hat{P}_Z^{(l-1)}(\ell) + c$ at each geocoordinate as a sampling weight, to obtain samples from $\hat{P}_{Z|X}^{(l)}(\ell)$. The realizations of x_i are given by the data. The constant c acts as an additional smoothing parameter and is set to $1 \cdot 10^{-10}$ in the Kernelheaping package.
- 4: M-Step: Estimate a new bandwidth \mathbf{H} using the samples from step 3, and use the samples and the new \mathbf{H} to compute the new KDE estimate of the current iteration, $\hat{P}_Z^{(l)}(\ell)$.
- 5: Repeat steps 2–4 for B (burn-in iterations) + L (additional iterations) times.
- 6: Discard the B burn-in density estimates and obtain the final density estimate of $P_Z(\ell)$ by averaging the remaining L density estimates $\hat{P}_Z(\ell)$ on the evaluation grid \mathbf{G} . The final estimate is called $P_{\text{GRSST}}(\ell)$.

It is crucial to observe that the full set of geocoordinates drawn in step 3 of Algorithm 1 is, depending on the granularity of \mathbf{G} , approximately equivalent to draws from $\hat{P}_Z^{(l)}(\ell)$. For each individual draw, x_i is nonstochastic; the scaling by the marginal likelihood $P_X(\ell)$ in the denominator of eq. (2.4) is accounted for by the relative empirical frequencies of the x_i in the sample. This is especially true in the case where $n = N$.

As already touched upon above, we can observe familiar structures from the EM algorithm in the GRSST algorithm, but there are significant differences, which we will highlight after a brief introduction to the core components of the EM family of algorithms. The EM algorithm assumes a fully specified parametric model $P_{Z,X}(z, x \mid \boldsymbol{\theta})$, with a latent variable Z , an observed variable X , and a vector of parameters $\boldsymbol{\theta}$. Given the parameters $\boldsymbol{\theta}^{(l)}$ of the current iteration l , the E-Step typically constructs a function

$$Q(\boldsymbol{\theta} \mid \boldsymbol{\theta}^{(l)}) = \int_{\Omega_Z} \log [P_{X,Z|\boldsymbol{\theta}}(x, z)] P_{Z|X,\boldsymbol{\theta}^l}(z \mid x) dz = \mathbb{E}_{Z|X,\boldsymbol{\theta}^{(l)}} [\log [P_{X,Z|\boldsymbol{\theta}}(x, z)]], \quad (2.6)$$

which is a lower bound of the log-likelihood $\log [P_{X|\boldsymbol{\theta}}(x)]$. The M-Step maxi-

mizes $Q(\boldsymbol{\theta} \mid \boldsymbol{\theta}^{(l)})$ with respect to $\boldsymbol{\theta}$ and thereby provides a new estimate $\boldsymbol{\theta}^{(l+1)}$ for the E-step of the next iteration. The resulting sequence $\boldsymbol{\theta}^{(0)} \dots \boldsymbol{\theta}^{(M)}$ monotonically increases towards local maxima or the global maximum of $\log [P_{X|\boldsymbol{\theta}}(x)]$. Convergence properties are studied in more detail by C. F. J. Wu (1983). Note that $P_{Z|X,\boldsymbol{\theta}^{(l)}}(z \mid x)$ can be interpreted as a weight for each data point, describing the association of each value of the observed value x with each possible value z given the current parameter estimate $\boldsymbol{\theta}^{(l)}$. These weights enable the appropriate consideration of the current estimate of the distribution of the latent variable z in the subsequent M-Step. For some scenarios, the integration over z in the E-step is prohibitively difficult or impossible. The Monte-Carlo EM algorithm, introduced by Wei and Tanner (1990), approximates $Q(\boldsymbol{\theta} \mid \boldsymbol{\theta}^{(l)})$ by

$$Q(\boldsymbol{\theta} \mid \boldsymbol{\theta}^{(l)}) \approx \frac{1}{T} \sum_{t=1}^T \log [P_{X,Z|\boldsymbol{\theta}}(x, \tilde{z}_t)], \quad (2.7)$$

where z_t denotes samples drawn from the current estimate of $P_{Z|X,\boldsymbol{\theta}^{(l)}}(z \mid x)$. So, instead of weighting with the current value of $P_{Z|X,\boldsymbol{\theta}^{(l)}}(z \mid x)$, T many pseudo-samples of z , denoted \tilde{z}_t , are drawn for each observed x , and the average joint log-likelihood is computed. A special case of the Monte-Carlo EM (MCEM) algorithm for a finite mixture model arises for $T = 1$ and is called the SEM algorithm (Celeux, 1985). The M-Step is replaced by the stochastic step (S-Step). The randomness introduced in the S-step causes the sequence of parameter estimates $\boldsymbol{\theta}^{(l)}$ to not converge monotonically towards the closest saddle point, plateau, or local maximum. Celeux et al. (1996) argue that the sequence $\boldsymbol{\theta}^{(l)}$ is an irreducible, time-homogeneous Markov chain when $P_{Z|X,\boldsymbol{\theta}^{(l)}}(z \mid x)$ is positive for almost every $\boldsymbol{\theta}$ and z . If this sequence can be shown to be ergodic, it will converge to the unique stationary probability distribution ϕ of the Markov chain. A natural candidate for an estimator of $\boldsymbol{\theta}$ is the average of the last L draws from the chain; see e.g., Nielsen (2000).

Coming back to the GRSST algorithm, we observe that, disregarding the logarithm in eq. (2.7), step 3 in Algorithm 1 is comparable to the S-Step in the SEM algorithm. Using the model's state from the previous iteration, $\hat{P}_Z^{(l-1)}(\boldsymbol{\ell})$, the algorithm completes the dataset by drawing samples from $P_{Z|X}^{(l)}(\boldsymbol{\ell}|x_i) \propto P_{X|Z}(x_i|\boldsymbol{\ell}) \hat{P}_Z^{(l-1)}(\boldsymbol{\ell})$. The model defined in eq. (2.2)–eq. (2.4) does not make explicit parametric assumptions about the distribution of Z . Instead of producing a sequence of parameter estimates $\boldsymbol{\theta}^{(l)}$, the algorithm generates a sequence of KDE estimates, $\hat{P}_Z^{(l)}(\boldsymbol{\ell})$. Therefore, the draws in the GRSST's S-Step differ from the classic SEM because $P_{Z|X}(\boldsymbol{\ell}|x_i)$ is constructed using last iteration's $\hat{P}_Z(\boldsymbol{\ell})$, unlike last iteration's

$P_{Z|X,\theta}(\ell)$ in the classic SEM. This general absence of parametric assumptions also affects the GRSST's M-Step. Instead of maximizing the (average, approximate) joint likelihood as in the EM, MCEM, or SEM algorithms, the GRSST algorithm minimizes the asymptotic mean integrated squared error of the kernel density estimator. The replacement of likelihood maximization with a surrogate function is a concept already applied in several generalizations of the EM algorithm (see e.g., Elashoff and Ryan (2004)). McLachlan and Krishnan (2007, ch. 7.7) provide an overview of the MM algorithm, which stands for Majorization-Minimization or Minorization-Maximization algorithm, a family of algorithms more general than the EM. The MM algorithm also allows for minimization in its second step (M-Step), and depending on the underlying model, a host of different surrogate functions can be constructed using relationships such as the Cauchy-Schwarz or Jensen's inequalities. The core difference between the GRSST and the MM algorithm family is that the surrogate function in GRSST is the RMISE function, which is minimized with respect to the chosen bandwidth in the KDE as opposed to model parameters. A rigorous treatment of convergence is still missing in the literature but is beyond the scope of this paper. This is why we also rely on simulation studies to judge the effectiveness of the AGRSST, just as in the original GRSST paper (Groß et al., 2016).

2.2 The Augmented Groß–Rendtel–Schmid–Schmon–Tzavidis Estimator

The precision of the GRSST estimator is naturally constrained by the size of geographical areas which determine the sets $\{A_1, \dots, A_d, \dots, A_D\}$ (Groß, 2016). The algorithm does not require any additional information about the distribution inside the sets A_d . The AGRSST estimator is a heuristic which enables the use of an auxiliary density $P_{\text{AUX}}(\ell)$ aimed at improving the GRSST estimate $P_{\text{GRSST}}(\ell)$. Hereby, $P_{\text{AUX}}(\ell)$ is thought to be similar to $P_Z(\ell)$ due to theoretical considerations. A classical example, which we will investigate later on, is the distribution of human population $P_Z(\ell)$, where the distribution of nighttime light emissions is a natural candidate as an auxiliary density, because increased emissions of light may correlate with an increased human population. Both densities, $P_{\text{GRSST}}(\ell)$ and $P_{\text{AUX}}(\ell)$, can be thought of as imperfect estimations of the true distribution $P_Z(\ell)$. The density $P_{\text{GRSST}}(\ell)$ is imperfect because of the coarseness of the input data X , and $P_{\text{AUX}}(\ell)$ because of the generally unknown level of similarity between $P_Z(\ell)$ and $P_{\text{AUX}}(\ell)$. Algorithm 2 depicts the steps to obtain the AGRSST estimator $P_{\text{AGRSST}}(\ell)$.

The core idea of the AGRSST estimator is to create a weighted combination of the standard GRSST density and an auxiliary density $P_{\text{AUX}}(\ell)$, which on average

Algorithm 2 Augmented Groß–Rendtel–Schmid–Schmon–Tzavidis Estimator

- 1: Run the standard GRSST algorithm to obtain $P_{\text{GRSST}}(\ell)$.
- 2: Evaluate $P_{\text{AUX}}(\ell)$ and $P_{\text{GRSST}}(\ell)$ on a fine grid \mathbf{G} .
- 3: Calculate representative mean densities of $P_{\text{AUX}}(\ell)$ and $P_{\text{GRSST}}(\ell)$ on the level of A_d to obtain \mathbf{m}_{AUX} and $\mathbf{m}_{\text{GRSST}}$.
- 4: Calculate the correlation $\hat{\gamma} = \text{cor}(\mathbf{m}_{\text{AUX}}, \mathbf{m}_{\text{GRSST}})$.
- 5: If $\hat{\gamma} < 0$, invert $P_{\text{AUX}}(\ell)$ on \mathbf{G} by setting it to $\frac{\max[P_{\text{AUX}}(\ell)] - P_{\text{AUX}}(\ell)}{\sum_i [P_{\text{AUX}}(\ell)]}$.
- 6: Determine $P_Z^{\text{temp}}(\ell) = \hat{\gamma}P_{\text{AUX}}(\ell) + [1 - \hat{\gamma}]P_{\text{GRSST}}(\ell)$.
- 7: Define the geocoordinate counts per area as $c_d = \sum_{i \in n} \mathbb{1}(x_i = A_d)$.
- 8: Benchmark by sampling c_d geocoordinates in each A_d according to $P_Z^{\text{temp}}(\ell)$.
Run a KDE with these geocoordinates to obtain a final estimate $P_{\text{AGRSST}}(\ell)$.

produces a better estimate. This is because if $P_{\text{AUX}}(\ell)$ is unreliable, the estimate largely depends on the more robust GRSST. However, if $P_{\text{AUX}}(\ell)$ is similar to the true distribution $P_Z(\ell)$, the combined estimate benefits by giving $P_{\text{AUX}}(\ell)$ a higher weight. In this context, $P_{\text{GRSST}}(\ell)$ serves as a baseline estimate grounded in known (population) data, while $P_{\text{AUX}}(\ell)$ has the potential to represent certain aspects of $P_Z(\ell)$ much better than $P_{\text{GRSST}}(\ell)$.

However, it is generally not clear how close $P_{\text{GRSST}}(\ell)$ is to $P_Z(\ell)$, and as a result, it is also not clear how much weight should be put on it. For this problem we propose a basic heuristic of setting the weight on $P_{\text{AUX}}(\ell)$ to be equivalent to $\hat{\gamma} = \text{cor}(\mathbf{m}_{\text{AUX}}, \mathbf{m}_{\text{GRSST}})$, which is the correlation of $P_{\text{AUX}}(\ell)$ and $P_{\text{GRSST}}(\ell)$ on the level of the A_d geographical areas. The vectors \mathbf{m}_{AUX} and $\mathbf{m}_{\text{GRSST}}$ are of length D and contain the average densities of $P_{\text{AUX}}(\ell)$ and the GRSST input data (x_i) . We compute \mathbf{m}_{AUX} independently of the unit underlying the auxiliary data by taking the average of $P_{\text{AUX}}(\ell)$ evaluated at the gridpoints inside each A_d . Since the unit of the GRSST input data is always geocoordinate counts we can compute $\mathbf{m}_{\text{GRSST}}$ by dividing the geocoordinate counts per area by the actual geographical size of their corresponding areas A_d , so $c_d \cdot \text{size}(A_d)$. Using linear correlation has the advantage of offering a measure that is inherently constrained within the range of $[-1, 1]$, which makes it suitable as a weight of the convex combination $P_Z^{\text{temp}}(\ell) = \hat{\gamma}P_{\text{AUX}}(\ell) + [1 - \hat{\gamma}]P_{\text{GRSST}}(\ell)$. Depending on the nature of the auxiliary variable behind $P_{\text{AUX}}(\ell)$, the intermediate density $P_Z^{\text{temp}}(\ell)$ might lose some of the information contained in the GRSST input data. To correct for such distortions, step 8 benchmarks the process so that the final estimate $P_{\text{AGRSST}}(\ell)$ is derived from a set of geocoordinates that align with the overall proportions specified by the GRSST input data. In some settings, $P_{\text{AUX}}(\ell)$ might exhibit a negative correlation with $P_Z(\ell)$. For example, if $P_{\text{AUX}}(\ell)$ represents the density of trees, we might

expect a negative relationship with $P_Z(\ell)$ if it represents human population density. For such cases we propose a pragmatic inversion of $P_{\text{AUX}}(\ell)$ as seen in step 6 of algorithm 2. If $P_{\text{AUX}}(\ell)$ is deemed to be quite informative of $P_Z(\ell)$ a intuitive approach of obtaining an estimate that combines the information of the auxiliary density with the one from the GRSST input data is to sample c_d many geocoordinates in each A_d weighted by $P_{\text{AUX}}(\ell)$. This method is, apart from the missing addition of the smoothing parameter c in Algorithm 1's step 4, almost equivalent to setting $\hat{\gamma} = 1$ in the AGRSST. We decided to abstain from adding the constant c in order to not disturb the information of the auxiliary density. It is a natural alternative for the AGRSST; we refer to this estimator as AGRSST1 and denote its density by $P_{\text{AGRSST1}}(\ell)$, and also investigate it.

2.3 Obtaining Auxiliary Densities

In practice, $P_{\text{AUX}}(\ell)$ will often need to be derived from raster data measuring some physical quantity. Algorithm 3 outlines our recommended method for converting this raw raster data into the $P_{\text{AUX}}(\ell)$ density. While it's possible to skip step (3) in Algorithm 3 and directly use $w^{std}(\mathbf{g}_j)$ in the AGRSST, our simulations indicate that creating $P_{\text{AUX}}(\ell)$ from a smoothed density, rather than the raw standardized data, generally leads to a slightly lower RMISE. If the auxiliary data is also given by a (more granular) choropleth count map, then we recommend using the standard GRSST to obtain $P_{\text{AUX}}(\ell)$.

Algorithm 3 Obtaining $P_{\text{AUX}}(\ell)$ from raster data

- 1: Associate each grid point \mathbf{g}_j in \mathbf{G} with the raw data value $r(\mathbf{g}_j)$ of the corresponding raster cell it falls into.
- 2: Draw a sample from \mathbf{G} using $w^{std}(\mathbf{g}_j) = r(\mathbf{g}_j) \cdot (\sum_{\mathbf{G}} r(\mathbf{g}_j))^{-1}$ as a sample weight. The sample size needs to be sufficiently large and can be a scaled version of the population sample size $f \cdot n$.
- 3: Estimate a standard KDE on the sampled grid points resulting in $P_{\text{AUX}}(\ell)$.

3 Simulation

3.1 Simulation Setup

In this section, we present the setup of the Monte Carlo simulation study used to assess the performance of the estimators introduced in Section 2. We use the map of the German state of Bavaria, which is obtained from the German Federal Agency for Cartography and Geodesy (2024). The simulation is based on

$t \in \{1, 2, \dots, T = 400\}$ iterations. In each iteration, an artificial true Bavarian population density $P_Z(\ell)$ is simulated. $P_Z(\ell)$ is obtained by randomly drawing 80 times from the geocoordinates $\mathbf{g}_j \in \{(\ell_j^o, \ell_j^a) \in \mathbb{R}^2\}$ on the fine grid \mathbf{G} . These geocoordinates are stored in the vector $\boldsymbol{\mu}$, which is set to the location parameter of a Gaussian mixture, such that

$$P_Z^{(t)}(\ell) = \sum_{k=1}^K \pi_k \mathcal{N}(\ell \mid \mu_k, \Sigma_k), \quad \sum_{k=1}^K \pi_k = 1, \quad 0 \leq \pi_k \leq 1, \quad \Sigma_k = \begin{bmatrix} \sigma_{k1}^2 & 0 \\ 0 & \sigma_{k2}^2 \end{bmatrix}, \quad (3.1)$$

where the index $k \in \{1, 2, \dots, K = 80\}$ enumerates each Gaussian component. The diagonal elements of the covariance matrices Σ_k are also randomly drawn, π_k is set to 1/80. For each simulation run, we draw an artificial Bavarian population of $n = 250\,000$ from $P_Z^{(t)}(\ell)$ using \mathbf{G} . The geographical aggregation level for the GRSST is the German NUTS-3 district (Kreise) level. The input vector \mathbf{x} for the GRSST is obtained by mapping the drawn geocoordinates \mathbf{z} to the corresponding district A_d in which they are located. Figure 1 shows the simulated true density $P_Z^{(t)}(\ell)$ and the aggregated sampled geocoordinates on district level for an exemplary simulation run t .

We obtain the auxiliary density $P_{\text{AUX}}^{(t)}(\ell)$ by taking the true density as a baseline $P_Z^{(t)}(\ell)$ and adding normally distributed distortions with varying variances. Generally, the GRSST (AGRSST) is a method designed to produce relatively reliable results for input data of low quality, due to aggregation. Depending on the target variable at hand, also $P_{\text{AUX}}(\ell)$ might be derived from data that is only available in a spatially aggregated form. In the simulation, we therefore base $P_{\text{AUX}}(\ell)$ on the German municipality (Gemeinden) level. The German municipalities are nested within the NUTS-3 level. Algorithm 4 depicts the process applied to obtain $P_{\text{AUX}}^{(t)}(\ell)$ from $P_Z^{(t)}(\ell)$. Note that Algorithm 4 simply aggregates the true density, averages and standardizes it on the municipality level, draws geocoordinates according to these values, re-aggregates them on the municipality level, and applies a GRSST estimator on these aggregates to obtain a smooth density.

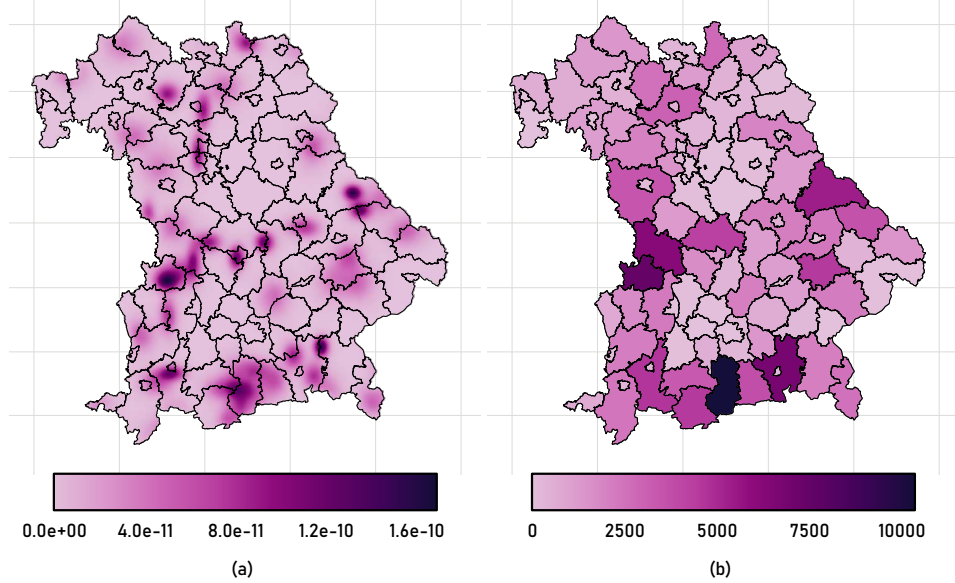


Figure 1: (a) Exemplary artificial Bavarian population density $P_Z^{(t)}(\ell)$ of an iteration run t and (b) the corresponding GRSST input data $\mathbf{x}^{(t)}$ resulting from 250 000 draws from $P_Z^{(t)}(\ell)$.

Algorithm 4 Obtaining $P_{\text{AUX}}^{(t)}(\ell)$ from $P_Z^{(t)}(\ell)$.

- 1: Denote the sets of geocoordinates that fall inside the p -th municipality with $\{Q_1, \dots, Q_p, \dots, Q_P\}$.
- 2: Evaluate $P_Z^{(t)}(\ell)$ on \mathbf{G} and calculate the mean density μ_{Q_p} of the grid points of \mathbf{G} inside every set Q_p , $\mu_{Q_p} = \sum_{\mathbf{g}_j \in Q_p} P_Z^{(t)}(\mathbf{g}_j) \left(\sum_{\mathbf{g}_j \in Q_p} \mathbf{1}_{\mathbf{g}_j \in Q_p}(\mathbf{g}_j) \right)^{-1}$.
- 3: Draw a sample (we chose the population size $n = 250 000$) from \mathbf{G} using $w_{\mu_{Q_p}}^{std}(\mathbf{g}_j \in Q_p) = \mu_{Q_p} \left(\sum_{\mathbf{g}_j \in \mathbf{G}} w_{\mu_{Q_p}}(\mathbf{g}_j \in Q_p) \right)^{-1}$ as a sample weight, where $w_{\mu_{Q_p}}(\mathbf{g}_j \in Q_p) = \mu_{Q_p}$.
- 4: Aggregate the samples drawn in step 3 to the municipality level $\{Q_1, \dots, Q_p, \dots, Q_P\}$.
- 5: Run the standard GRSST algorithm with the aggregates of the previous step, which returns $P_{\text{AUX}}^{(t)}(\ell)$.

To simulate auxiliary densities of different quality, we distort the μ_{Q_p} with nor-

mally distributed errors with different variances.

$$\mu_{Q_p, d} = \mu_{Q_p} + \epsilon_d, \quad \epsilon_d \sim \mathcal{N} \left(0, \left(d \cdot \mu_{Q_p} \cdot \left(\sum_{p=1}^P \mu_{Q_p} \right)^{-1} \right)^2 \right), \quad (3.2)$$

where the standard deviation of ϵ is set to the standardized average density over all the municipalities scaled by $d \in \{0, 0.5, 1, 2.5, 5, 10, 15, 20\}$. Replacing μ_{Q_p} with $\mu_{Q_p, d}$ in step 2 of Algorithm 4 leads to auxiliary densities of varying quality, denoted by $P_{\text{AUX}, d}^{(t)}(\ell)$.

Following Groß et al. (2016), the primary measure we use to judge the quality of an estimate $\hat{P}_Z(\ell)$ of $P_Z(\ell)$ is the RMISE, which we approximate with

$$\begin{aligned} \text{RMISE} \left(\hat{P}_Z(\ell) \right) &= \sqrt{\mathbb{E} \left[\int \left(P_Z(\ell) - \hat{P}_Z(\ell) \right)^2 dz \right]} \approx \sqrt{\frac{1}{m} \sum_{g \in \mathbf{G}} \left(P_Z(\mathbf{g}_j) - \hat{P}_Z(\mathbf{g}_j) \right)^2 \delta_{\mathbf{g}_j}^2} \\ &\propto \sqrt{\frac{1}{m} \sum_{g \in \mathbf{G}} \left(P_Z(\mathbf{g}_j) - \hat{P}_Z(\mathbf{g}_j) \right)^2}, \end{aligned} \quad (3.3)$$

the term δ refers to the side lengths of the square pixels, where the \mathbf{g}_j are the centroids. The grid is evenly spaced, with $\delta_{\mathbf{g}_j}^2$ being a scalar for all \mathbf{g}_j . In the rest of this paper, we refer to RMISE as the last term of eq. (3.3).

3.2 Simulation Results

In this section, we discuss the results obtained from the Monte Carlo simulation study laid out in the previous section. For the burn-in and additional iterations, we chose $B = 30$ and $L = 20$. Figure 2 depicts the behavior of $P_Z^{(t)}(\ell)$ at three different locations; one that showed high (medium, low) density in the first ($l = 1$) iteration of the algorithm. It can be seen that after the pilot iteration ($l = 0$), the densities seem to quickly reach a behavior that suggests that $P_Z^{(t)}(\ell)$ is roaming around the stationary distribution of the Markov chain (if it exists). Additionally, choosing $B = 30$ and $L = 20$ surpasses the recommendations in the supplementary material of Groß (2016). We therefore conclude that the chosen number of 50 iterations is sufficient in our context.

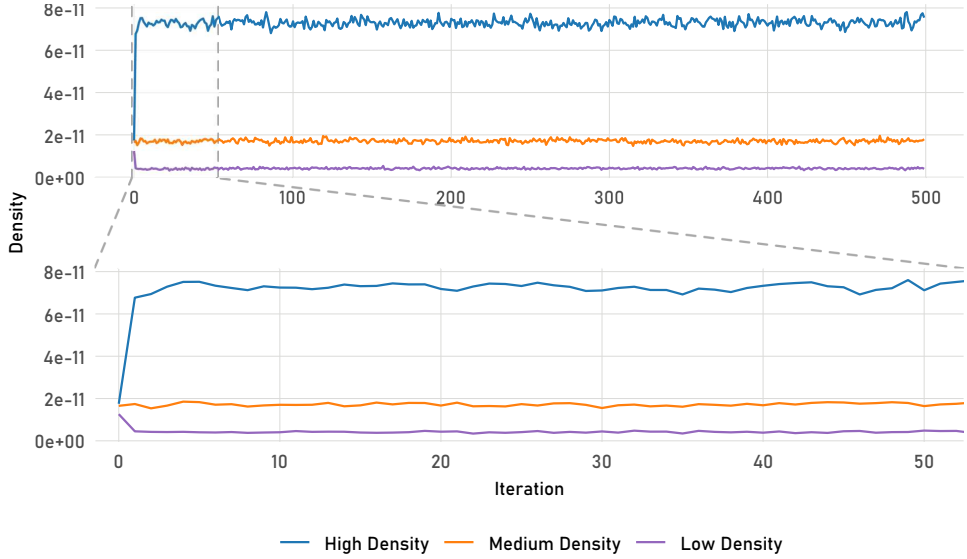


Figure 2: The development of $\hat{P}_Z^{(l)}(\ell)$ over $M = 1000$ iterations of the GRSST evaluated at 3 different g_j . Blue (purple, orange) represents a geocoordinate that displayed relatively high (medium, low) density in the first ($l = 1$) iteration. A zoomed-in view of the first 50 iterations is shown in the lower panel.

The boxplots in Figure 3 display the distribution of the RMISE across 400 simulation runs for each distortion level and estimator used: $P_{\text{GRSST}}(\ell)$, $P_{\text{AUX}}(\ell)$, $P_{\text{AGRSST}}(\ell)$, and $P_{\text{AGRSSTI}}(\ell)$. As expected, the RMISE of the GRSST estimator remains almost constant across different distortion levels, as it is completely independent of $P_{\text{AUX}}(\ell)$; minor differences can be attributed to sampling uncertainty. All estimates that utilize the auxiliary density $P_{\text{AUX}}(\ell)$ perform significantly better than the GRSST for low levels of distortion. This advantage diminishes and even reverses in the case of $P_{\text{AGRSSTI}}(\ell)$ with increasing levels of distortion. The auxiliary density $P_{\text{AUX}}(\ell)$ behaves as anticipated: since it is obtained via a GRSST on the municipality level, its RMISE is lower than that of the GRSST on the district level. At elevated levels of distortion, $P_{\text{AUX}}(\ell)$ is derived from samples of a density that exhibits increasing divergence from the true density $P_Z(\ell)$. Consequently, its RMISE is generally much higher than that of the GRSST estimator. The poor performance of $P_{\text{AUX}}(\ell)$ at high distortion levels highlights how, in practice, simply choosing a seemingly similar density as an estimate for another should be avoided.

The methods that utilize the GRSST input data ($P_{\text{AGRSST}}(\ell)$ and $P_{\text{AGRSSTI}}(\ell)$) mitigate the effects of a very poor auxiliary density. The comparison between $P_{\text{AGRSST}}(\ell)$

and $P_{\text{AGRSSTI}}(\ell)$ reveals lower RMISE values for the AGRSST at both the lowest and high distortion levels, whereas $P_{\text{AGRSSTI}}(\ell)$ outperforms the AGRSST for moderate distortions. For highly informative auxiliary densities where the only source of divergence from the true density is the averaging at the municipality level (distortion = 0), the benchmarking step in $P_{\text{AGRSST}}(\ell)$ and $P_{\text{AGRSSTI}}(\ell)$ does not improve the estimate but increases it due to the noise from the additional KDE process. In practice, this effect would only be relevant for auxiliary densities that are very similar to the true density and is therefore of little practical consequence. The AGRSST's advantage over the AGRSST1 at zero distortion likely stems from its ability to assign a small weight to the GRSST estimate, which slightly smooths the municipality-level based $P_{\text{AUX}}(\ell)$. In the case of moderate distortions (100 - 500), the additional information about the true density incorporated into $P_{\text{AGRSSTI}}(\ell)$ outweighs this advantage, and $P_{\text{AGRSSTI}}(\ell)$ outperforms $P_{\text{AGRSST}}(\ell)$. For very poor auxiliary densities, AGRSST performs better than $P_{\text{AGRSSTI}}(\ell)$ due to its ability to assign weight to the GRSST estimate, which is superior and more conservative because of its independence from the (heavily distorted) auxiliary density.

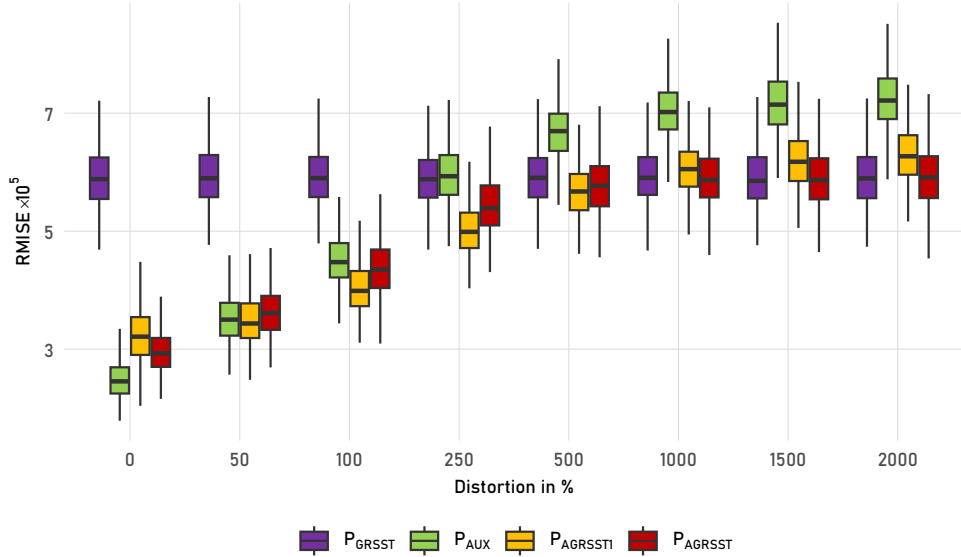


Figure 3: Boxplots of the RMISE of $P_{\text{GRSST}}(\ell)$, $P_{\text{AUX}}(\ell)$, $P_{\text{AGRSST}}(\ell)$ and $P_{\text{AGRSSTI}}(\ell)$ over increasing levels of distortion of $P_{\text{AUX}}(\ell)$.

The above described behavior is confirmed by Figure 4, which shows the dependence of $\hat{\gamma}$ on the distortions. We deem the displayed relationship between $\hat{\gamma}$ and

the distortion levels as generally desirable, because it drives the advantages of the AGRSST illustrated in Figure 3. Though, when examining the interplay between the true density $P_Z(\ell)$, $P_{\text{AUX}}(\ell)$ and $\hat{\gamma}$ the limitations of the AGRSST become apparent. The performance of the AGRSST estimator relies on the fact that $\hat{\gamma}$ properly reflects the similarity between the true- and the auxiliary density. Confounding factors that can negatively impact the reflection of this relationship via $\hat{\gamma}$ can be:

- Nonlinearity: $P_Z(\ell)$ and $P_{\text{AUX}}(\ell)$ might be related in a nonlinear fashion. Since $\hat{\gamma}$ is essentially a standard empirical correlation, it might not, or only partly, capture such relationships.
- Ecological fallacy (Holt et al., 1996): Since all the information about $P_Z(\ell)$ is limited to the GRSST input data at its respective geographical aggregation level, we calculate $\hat{\gamma}$ at that level. The AGRSST assumes, though, that $\hat{\gamma}$ is a valid similarity measure at the level of the densities.

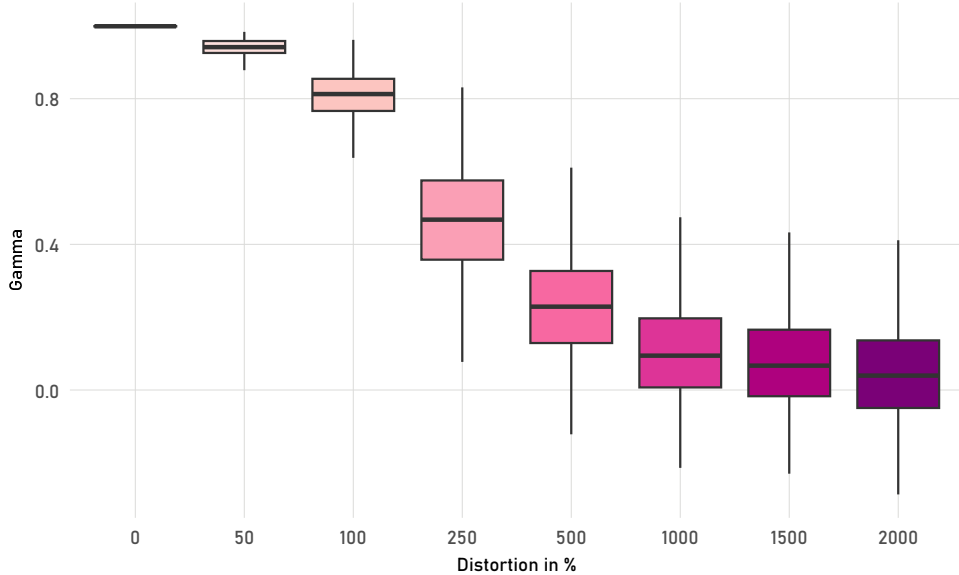


Figure 4: Boxplots of the calculated value of $\hat{\gamma}$ over increasing levels of distortion of $P_{\text{AUX}}(\ell)$.

The main tool to counteract problems caused by a $\hat{\gamma}$ that does not reflect the quality of $P_{\text{AUX}}(\ell)$ is the benchmarking (step 8 in Algorithm 2). It limits the amount of possible divergence of $P_{\text{AGRSST}}(\ell)$ from $P_{\text{GRSST}}(\ell)$. The worst-case scenario for the AGRSST is a highly divergent auxiliary density from the true density, which

is still highly correlated with the true density at the GRSST input level. This scenario is covered by our simulation study; at the highest distortion levels, $P_{\text{AGRSSTI}}(\ell)$ puts maximum weight on very poor auxiliary densities ($\hat{\gamma} = 1$). We observe that $P_{\text{AGRSSTI}}(\ell)$ performs worse than the GRSST, but the benchmarking step still ensures that divergence is limited. The AGRSST is basically equivalent to the GRSST at these high distortion levels. The main insights from our simulation study are that:

- $P_{\text{AGRSSTI}}(\ell)$, which benchmarks a plausible auxiliary density with the GRSST input c_d , is an attractive alternative to the GRSST with large potential gains in RMISE but a potentially worse RMISE for poor auxiliary densities.
- In contrast to $P_{\text{AGRSSTI}}(\ell)$, the AGRSST provides another layer of security to practitioners by limiting the weight placed on the auxiliary density when low correlation at the GRSST input level is detected. The trade-off for this increased security is a lower RMISE performance in the case of very informative auxiliary densities.

4 Evaluation Study on Population Data

4.1 Target Variable

The estimation of human population distributions is a classic area of interest in research in order to allow for targeted social- and environmental planning and policy development. Multiple contributions to the topic are, for example, added by the WorldPop research group; see, e.g., Stevens et al. (2015) or Sorichetta et al. (2015). In our first application, we use recently published data from the German Census 2022 that is conducted by the Federal Statistical Office of Germany (Destatis). Population counts are available in 100-meter raster cells (Destatis, 2024b) and also at the district level (Destatis, 2024a). We consider the raster data in relation to the size of Bavaria as granular enough to estimate a density $P_Z(\ell)$, which we assume to be the true population distribution. This density is estimated using a KDE based on geocoordinates located at the centroids of each raster. So, for a raster XYZ in which X-many people live, we place X-many geocoordinates at the centroid of XYZ. This is done for all rasters in Bavaria. The true distribution $P_Z(\ell)$ follows from a KDE on the resulting dataset (Figure 5 panel (a)). We obtain $P_{\text{GRSST}}(\ell)$ by running the GRSST estimator on the district-level population data (Figure 5 panel (b)). Since highly accurate data on the population distribution is already available, the principal objective of our first application is not to obtain an even more accurate estimate of the population density, but to use and compare our methods in a real-world scenario in which we also have access to a fairly accurate estimate of the ground truth $P_Z(\ell)$.

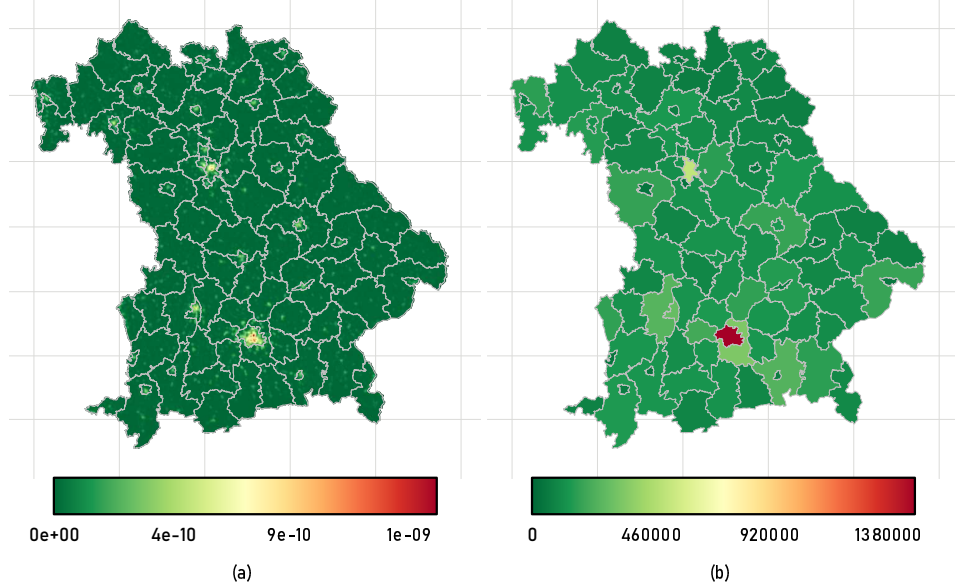


Figure 5: (a) The assumed ground truth, a KDE of the true Bavarian population based on the 2022 German Census 100 meter raster data and (b) the Bavarian population on the NUTS-3 district (Kreise) level, which serve as the GRSST input data.

4.2 Auxiliary Variable

In practice, the auxiliary density $P_{\text{AUX}}(\ell)$ can be derived from various sources with differing underlying units and aggregation levels. For example, in the case of nighttime light satellite raster data (Elvidge et al., 2021) that we use, the resolution of 15 arc-seconds (≈ 300 meters at the latitude of Bavaria’s geographical center) is fairly granular with respect to the sizes of the NUTS-3 districts. In this example, the radiance of the light is measured in watt per steradian per square meter ($W \cdot sr^{-1} \cdot m^{-2}$). For our application, we use the 2022 masked median radiance from monthly averages. The process to obtain these values includes multiple steps to adjust for distortions such as biomass burning or aurora and is documented in Elvidge et al. (2021). The general relationship between nighttime lights and population density is well established and, e.g., studied by Sutton (1997), Elvidge et al. (1999), Sutton et al. (2001), B. Wu et al. (2023).

In the scope of Bavaria, we deem the resolution of nighttime light radiance data granular enough to directly convert it into a density using Algorithm 3. Depending on the target variable at hand, the analyst might not have access to auxiliary data as granular as the nighttime light satellite data. In such cases, we recommend

using a GRSST for the conversion, similar to Algorithm 4. As the sample size in Algorithm 3, we chose the unscaled Bavarian population ($n = 13\,038\,724$). Note that the analyst can scale this number, if computational resources allow, to further reduce the sampling uncertainty, although the gains are likely to be relatively small given the already large sample size. The smoothing effect by the KDE can be judged visually by comparing the (transformed) raw data to $P_{\text{AUX}}(\ell)$ as in Figure 6. If core features of the raw data are smoothed out, we recommend using the raw data or increasing n . The benchmarked auxiliary density $P_{\text{AGRSST1}}(\ell)$ is analogously obtained from $P_{\text{AUX}}(\ell)$ as in the simulation study.

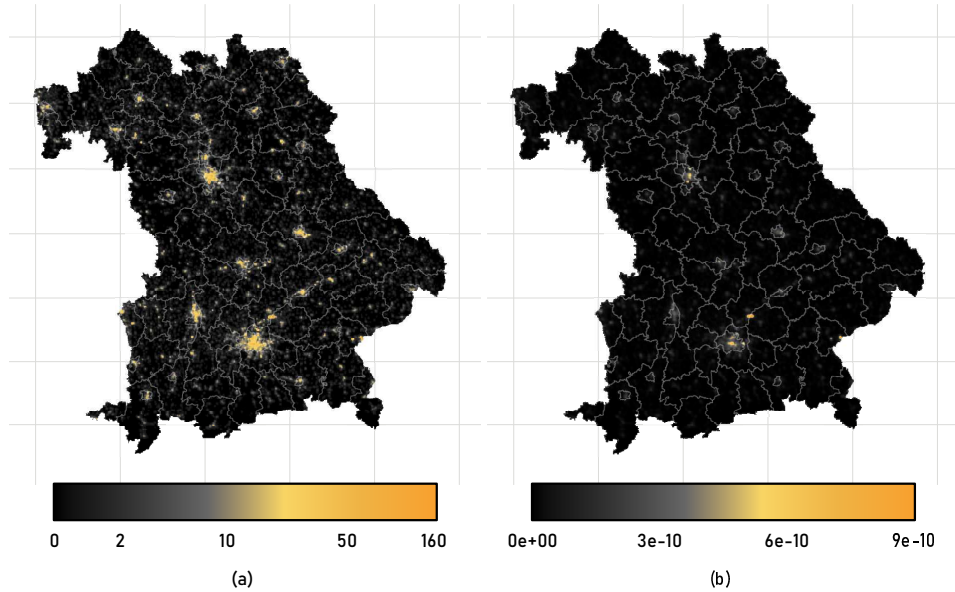


Figure 6: (a) The raw nighttime light satellite raster data, displayed on a pseudo log-transformed color scale for better contrast, and (b) the auxiliary density $P_{\text{AUX}}(\ell)$ derived by Algorithm 3. The auxiliary density is also pseudo log-transformed, and values above $9 \cdot 10^{-9}$ (located at Munich airport) are cut for improved visibility.

4.3 Evaluation Results

The value for γ is calculated as laid out in Section 2.2 and is $\hat{\gamma} \approx 0.945$, which means that the light density values are highly correlated with the Bavarian population densities at the district level. The availability of the true density allows us to determine RMISE values, which are depicted in Table 1.

Compared to the simulation study, the improvements of the AGRSST over the

Method	RMISE $\cdot 10^5$
$P_{\text{GRSST}}(\ell)$	8.3252
$P_{\text{AGRSST1}}(\ell)$	8.1803
$P_{\text{AGRSST}}(\ell)$	8.1396
$P_{\text{AUX}}(\ell)$	8.8786

Table 1: RMISE values of the different population density estimates, calculated based on census population data.

GRSST in this real-world example appear rather small, with a RMISE reduction of 2.23%. A potential reason for such small gains could be large deviations between light intensity and actual population in areas such as airports or the at Theresienwiese in Munich (Figure 8). Interestingly, the AGRSST1 performs slightly worse than the AGRSST; we attribute this to the additional smoothing that the mixture provides, especially in said areas with large deviations between light and population density, a dynamic that we also observed in our simulation study at the zero distortion level. The non-benchmarked $P_{\text{AUX}}(\ell)$, in turn, has a 6.65% higher RMISE than the GRSST. This structure can be compared to the distortion levels of 250 and 500 in our simulation study, where the AGRSST and AGRSST1 outperform the GRSST, even with an auxiliary density that itself has a higher RMISE than the GRSST. Figure 7 depicts the resulting densities; upon visual inspection, the large-scale population density seems to be much better captured by AGRSST and AGRSST1, contrary to the small improvement in RMISE.

Figure 8, an enlarged view of Figure 7 focusing on Munich, illustrates the dynamics of all three methods. While the GRSST estimate appears largely uniform within Munich’s boundaries, AGRSST1 and AGRSST manage to capture some of the true population dynamics, although both incorrectly depict the Theresienwiese area in central Munich – the site of the famous Oktoberfest – as having the highest density, rather than a low population. Given the relatively spiky nature of the auxiliary density, the more conservative nature of AGRSST compared to AGRSST1 is evident in its less spiky density. This example highlights the significant dependence of the AGRSST on the auxiliary density and underscores the importance of selecting these densities based on expert subject knowledge. Despite the generally limited data availability typically associated with GRSST usage, our overall evaluation study demonstrates the potential of AGRSST to enhance GRSST density estimates, both in terms of RMISE and visual representation.

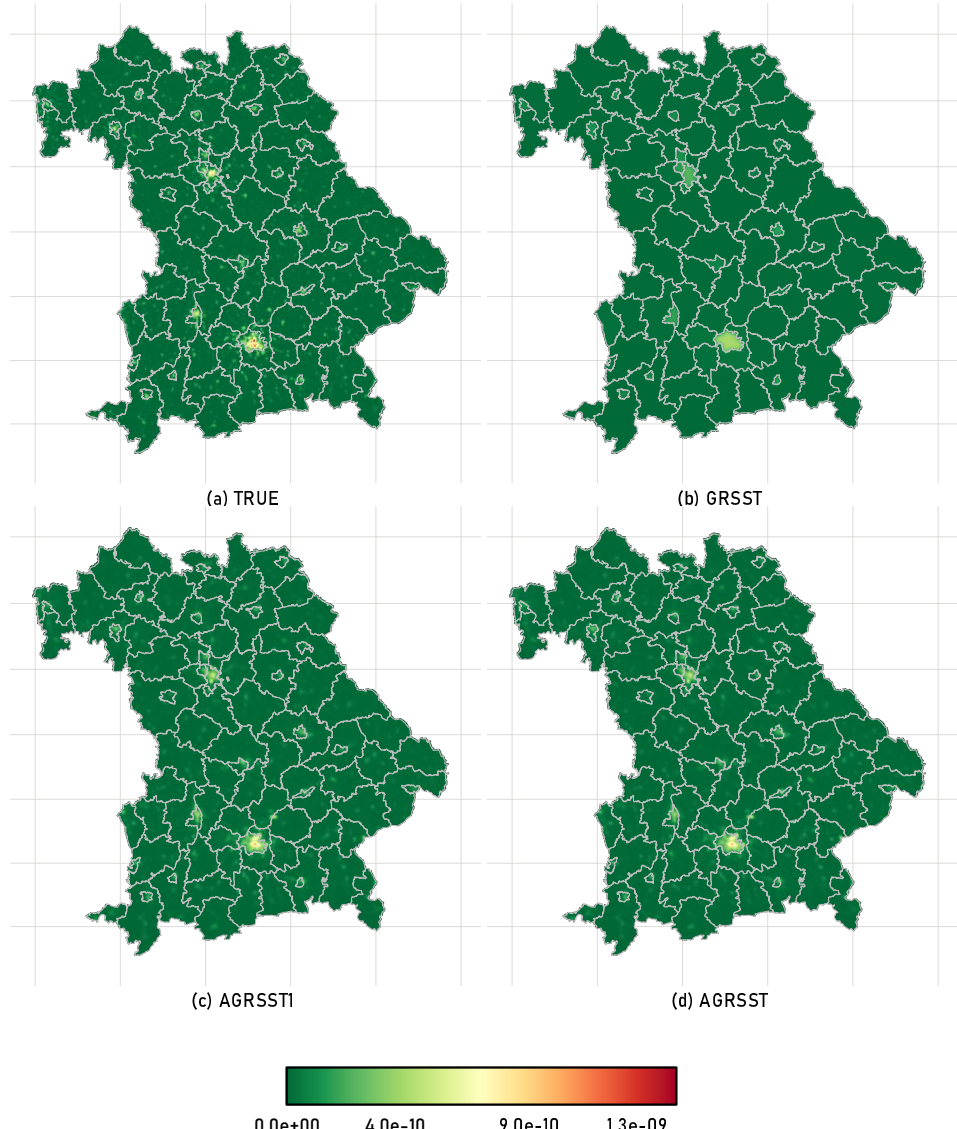


Figure 7: (a) The assumed ground truth, a KDE of the true Bavarian population based on the 2022 German Census 100-meter raster data, (b) the GRSST- , (c) AGRSST- and (d) the AGRSST1 estimate.

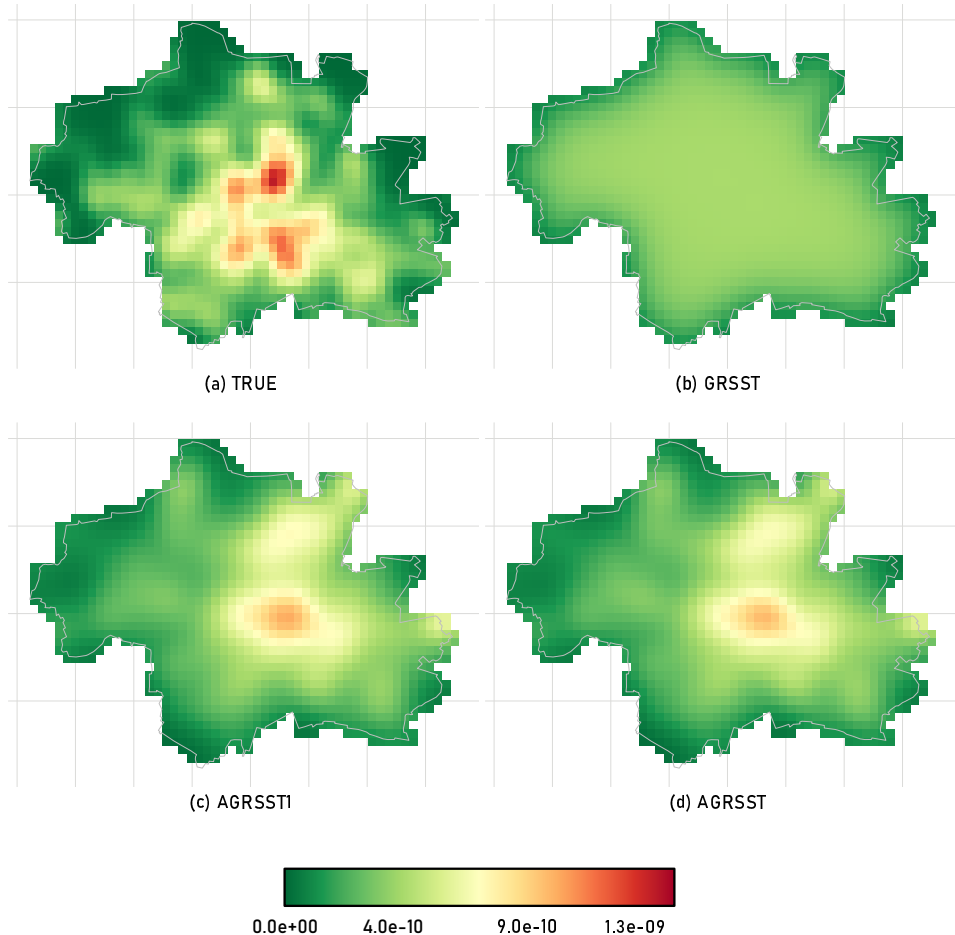


Figure 8: (a) The assumed ground truth, a KDE of Munich's true population based on the 2022 German Census 100-meter raster data, (b) the GRSST- , (c) AGRSST- and (d) the AGRSST1 estimate.

5 Application Rabbit Population Control

5.1 Target Variable

The *Lepus europaeus*, often called the brown hare or European hare, is a species of *Lepus* that is native to many European countries but has also been introduced into areas all over the world. Bock (2020) provides a comprehensive overview and literature collection on the general characteristics, distribution, ontogeny, reproduction, and other aspects of the mammal. Since the 1960s, there has been a steep decline in brown hare populations across Europe. The primary causes of this decline are believed to be the loss of landscape diversity and the emergence of diseases (see e.g., Smith et al. (2005)). Since 2015, the population of brown hares in Lower Saxony has shown signs of recovery, which is likely attributable to the dry conditions experienced in recent years, which have resulted in a decline in infection rates. The implementation of local initiatives by hunters, including the creation of wildflower strips and increased predator hunting, is another potential contributing factor to the recovery (Gräber et al., 2024). Sliwinski et al. (2019) studied the influence of different habitat variables on brown hare population density in Lower Saxony, using generalized additive mixed models (GAMMs) fit at the municipality level. We focus on identifying areas of high and low hunting intensity. To achieve this, we estimate a density based on the number of brown hares killed per district in Lower Saxony and Bremen during the hunting season 2023/2024 (01.04.2023 - 31.03.2024) (Dammann-Tamke, 2025). The number of animals killed by hunting and/or traffic-related accidents is also referred to as the hunting bag or hunting bag statistic. While hunting bag statistics have been used as a proxy to infer trends in wildlife population densities, this practice is not always advisable for reasons such as temporary hunting bans (Gräber et al., 2024). As a complement to wildlife population densities, hunting bag statistics are still an important analytical tool used to determine overall variations in wildlife numbers (see e.g., Havet (2002)) and are needed to implement harvest management schemes (Aubry et al., 2020).

5.2 Auxiliary Variable

We utilize the NDVI as the underlying data for the purpose of obtaining an auxiliary density for the hunting bag data. The fundamental concept (see Huete et al. (2002)) underpinning vegetation indices, such as the NDVI, is based on the study of the spectral reflectance of leaves. The reflected radiation in the red band from leaves is relatively low due to the absorption of light by photosynthetically active pigments, such as chlorophyll. In contrast, a significant portion of near-infrared radiation (NIR) is reflected, primarily due to the internal structure of plant leaves. This

contrast between red and near-infrared reflectance allows for the construction of the NDVI as a sensitive index used to quantify vegetation, given by

$$NDVI = \frac{\rho_{\text{NIR}} - \rho_{\text{RED}}}{\rho_{\text{NIR}} + \rho_{\text{RED}}}. \quad (5.1)$$

where ρ_{NIR} and ρ_{RED} are the surface bidirectional reflectance factors in the near-infrared and red bands. The raw data is collected by the moderate resolution imaging spectroradiometer (MODIS) on board the Earth Observing System-Terra platform (Didan & Barreto-Muñoz, 2019). We use the MOD13A1 : 16-day 500m VI data product (Didan, 2021), which provides 500-meter NDVI raster data in 16-day intervals. The specified interval (01.04.2023 - 31.03.2024) encompasses a total of 23 timestamps for raster layers. The mean of these raster values is calculated, resulting in a single NDVI raster layer for the designated hunting season (2023/2024). The NDVI is standardized between -1 and 1, with the majority of observed values falling between 0 (water or bare soil) and 0.8 (dense vegetation). Panel (a) in Figure 9 displays the NDVI raw data over Lower Saxony. There is a rich body of literature (e.g., Sliwinski et al. (2019), Schai-Braun et al. (2012), Smith et al. (2005)) on brown hare habitat preferences, which indicates that these depend on factors such as season, temperature, precipitation, and brown hare density itself. Generally, we can conclude that brown hares prefer heterogeneous agricultural landscapes with a mix of crops, grasslands, and semi-natural habitats, avoiding large monocultures, urban areas, and intensively farmed regions. The NDVI does not directly reflect all of these factors, such as agricultural heterogeneity, but the general assumption of a positive relationship between vegetation, expressed by NDVI, and the brown hare hunting bag seems plausible.

5.3 Application Results

Applying the steps outlined in Section 2.2 again yields a value of $\hat{\gamma} \approx 0.2067$, indicating a rather low, yet still significant correlation between NDVI and the brown hare hunting bag. The resulting density estimates are displayed in Figure 10. Unlike our evaluation study in the preceding section, it is not possible to determine RMISE values here because the brown hare hunting bag data is only available at the district level. Panel (a) of Figure 10 illustrates the auxiliary density $P_{\text{AUX}}(\ell)$ derived from the raw NDVI data. It is important to note that panel (a) has its own distinct color scale and legend, whereas panels (b)-(d) share a common color scale to facilitate comparisons. The figure reveals that the auxiliary density is relatively flat compared to the GRSST. From the global perspective provided by Figure 10, we can observe the typical behavior of GRSST, exhibiting a rather smooth density within districts. In contrast, AGRSST1 and AGRSST display more structure within

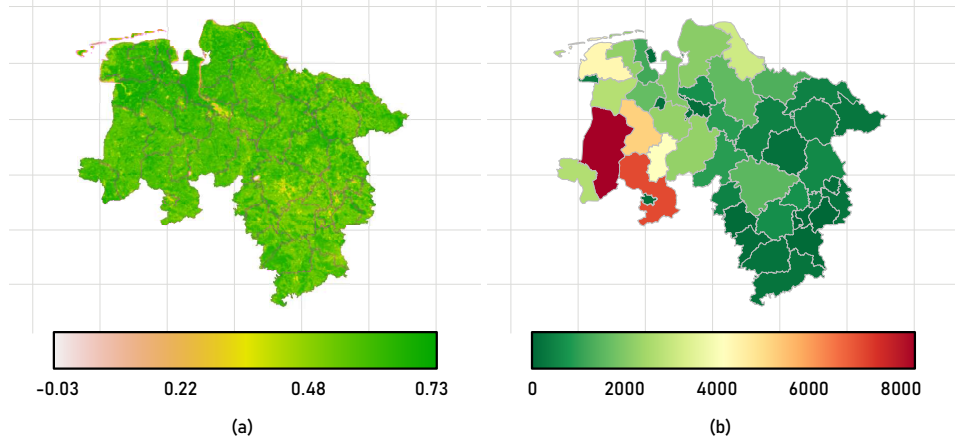


Figure 9: (a) The NDVI and (b) brown hare hunting bag data of Lower Saxony during the hunting season 23/24. The borders display the German NUTS-3 district (Kreise) level.

these districts. All three estimators indicate a west-to-east gradient with high bag densities in the west and declining densities to the east. In contrast to the absolute bag data (panel (b) in Figure 9), the KDE-based estimators identify a cluster of brown hare hunting in the three districts of Vechta, Cloppenburg, and Osnabrück, with Vechta being the district exhibiting by far the highest bag density. Figure 11 zooms in on the district of Vechta to better visualize the discrepancies between the three estimates; the color scales remain consistent.

The AGRSST1 significantly reflects some of the structure of the auxiliary density shown in panel (a); the dark green high vegetation hotspots north and south of Vechta can be clearly identified. Note that we observed a much larger impact of the auxiliary density in our evaluation study. The limited effect of the NDVI is due to two characteristics of the input data. First, the total count of $n = 64\,779$ causes the determinants of the bandwidth matrices \mathbf{H} to be relatively large compared to the setting in our evaluation study, which in turn causes the resulting density estimates to be smoother. Second, the NDVI auxiliary density is generally much smoother than the GRSST density, which is quickly confirmed by comparing the maximum values: $2.5 \cdot 10^{-11}$ for the auxiliary density versus $8.0 \cdot 10^{-11}$ for the GRSST. Also, contrary to our expectation, the AGRSST estimate seems to have higher maximum density values than the AGRSST1 and the GRSST. Two factors contribute to this: first, the AGRSST's derivation without the additional constant in step 3 of Algorithm 1 results in a spikier estimate compared to the GRSST; second, the relatively flat auxiliary density leads to a flatter AGRSST1 estimate.

Considering these aspects, we prefer the AGRSST1 approach for this particular application, as it is sensitive to the NDVI input data while maintaining a high degree of smoothness. This balance already helps limit potential errors compared to the GRSST, even without relying on the AGRSST rationale.

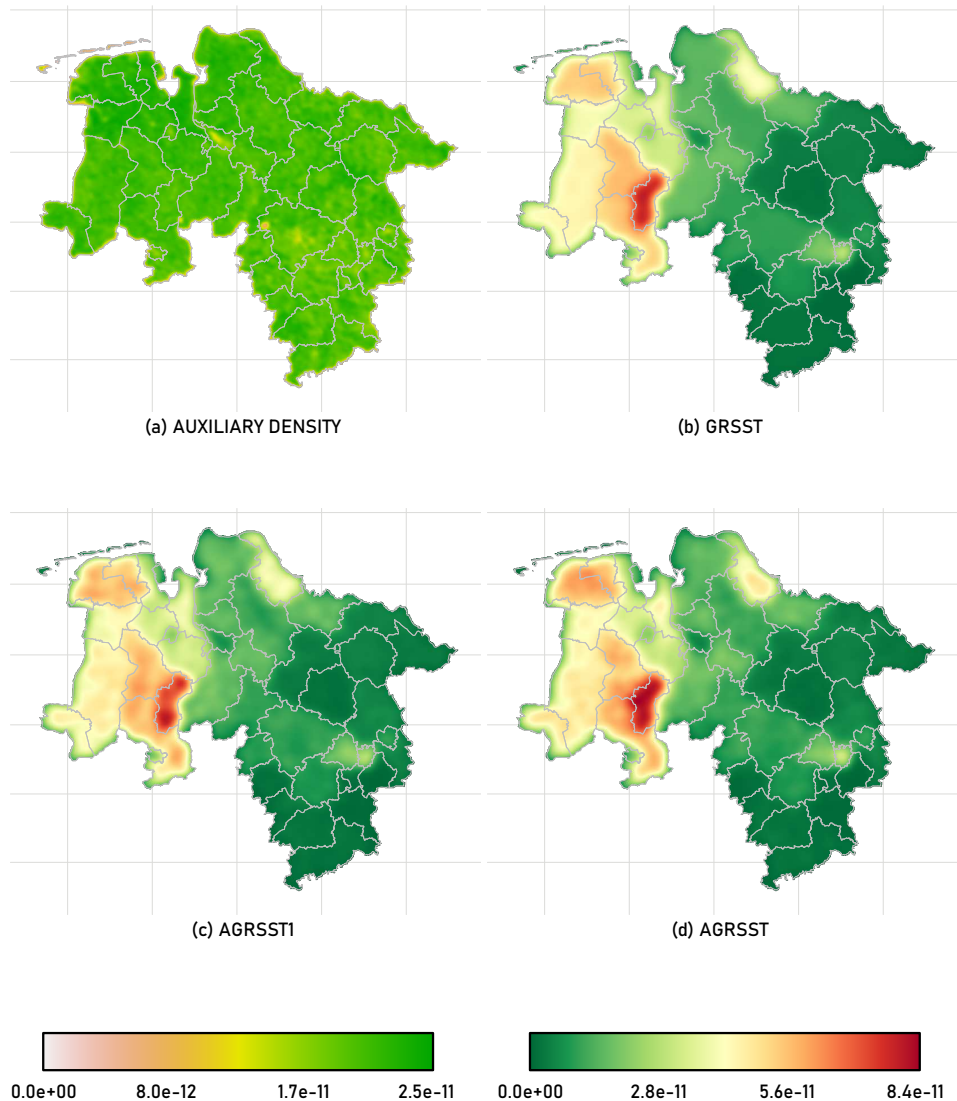


Figure 10: (a) The auxiliary density, obtained by applying Algorithm 3 on the raw NDVI data (the corresponding color scale is on the bottom left), (b) the GRSST, (c) AGRSST, and (d) the AGRSST1 estimate (their color scale is on the bottom right).

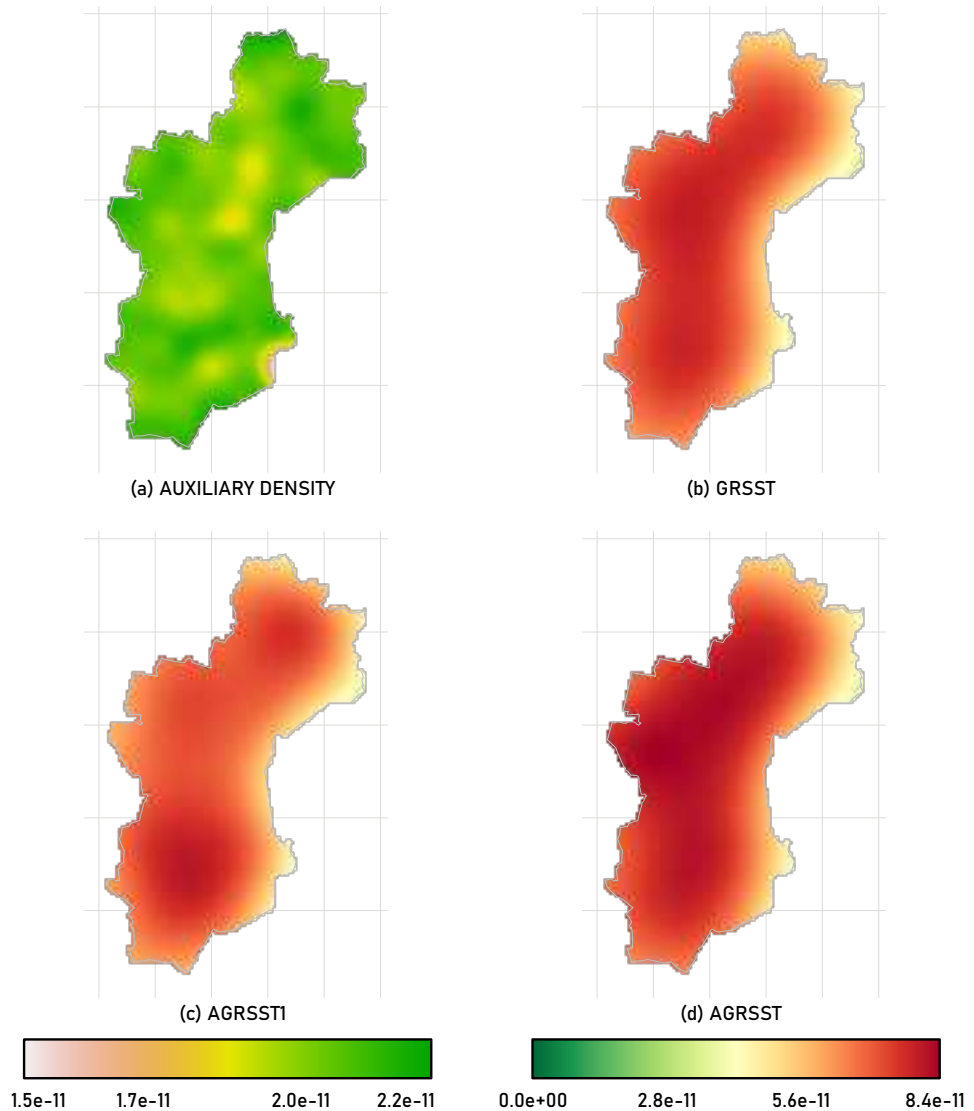


Figure 11: A version of Figure 10, zoomed-in on the district of Vechta. (a) The auxiliary density, obtained by applying Algorithm 3 on the raw NDVI data (the corresponding color scale is on the bottom left), (b) the GRSST, (c) AGRSST, and (d) the AGRSST1 estimate (their color scale is on the bottom right).

6 Conclusion

In this paper, we propose an extension to the GRSST estimator, which we name AGRSST. The GRSST is a method that broadens the applicability of KDE to challenging scenarios involving aggregated data, enabling more profound insights compared to basic choropleth maps displaying absolute counts. These advantages include facilitating the identification of spatial clusters and enabling the transformation of area aggregates between non-hierarchical geographical systems. However, the inherent accuracy of the GRSST remains limited by the relative geographical size of its input areas, as no direct information about the density distribution within these areas is provided.

The AGRSST estimator linearly combines the auxiliary and GRSST densities. The weight assigned to the auxiliary density is determined by its correlation with the GRSST-derived density at the level of the aggregated spatial units. This allows the AGRSST to adapt to the informativeness of the auxiliary data, placing more emphasis on it when it exhibits a strong positive correlation and relying more on the conservative GRSST estimate when the correlation is weak. Furthermore, a benchmarking step ensures that the final density estimate is based on the original aggregated counts. We also highlighted a special version of the AGRSST, the AGRSST1, which directly samples within the aggregated units according to the auxiliary density.

To evaluate the effectiveness of the AGRSST estimator, we conducted simulation study using the administrative map of Bavaria, Germany. We simulated various true population densities and generated auxiliary densities of varying quality by introducing controlled levels of distortion. The RMISE was used as the primary metric to assess the performance of the standard GRSST and the proposed AGRSST variants across these different distortion levels. The results of our simulation study show that depending on the quality of the auxiliary density large accuracy improvements are possible when using the AGRSST. It also became apparent that the correlation based convex combination serves as a mechanism which limits the negative influences of poor auxiliary densities. When fully weighting the auxiliary density (AGRSST1), we observe the potential for greater improvements over the GRSST, but also the risk of worse estimates in terms of RMISE, contingent on the quality of the auxiliary density. These findings are corroborated in a real-world evaluation using German Census data and remotely sensed nighttime lights, where, owing to the high correlation between nighttime lights and population density, AGRSST1 outperforms AGRSST, which in turn outperforms the GRSST.

Lastly, applying AGRSST and AGRSST1 to Lower Saxony's brown hare hunting bag data reveals a west-to-east density gradient, with intense hunting clus-

tered in the Vechta, Cloppenburg, and Osnabrück districts. Comparing the estimators, AGRSST is spikier than GRSST, while only AGRSST1 effectively integrates information from the NDVI data. Considering these factors, we conclude that AGRSST1 is the preferred method for this application.

The findings of this paper open several interesting avenues for future research in this domain. A potentially powerful enhancement could involve the integration of auxiliary densities within each iteration of the GRSST algorithm. Indeed, during the course of this research, we explored one such approach, wherein the standard KDE step in the GRSST was replaced by weighted KDE (see, e.g., Wang and Wang (2007)), with weights determined by the corresponding values of the auxiliary density at the locations of the input geocoordinates. Unfortunately, this specific implementation did not yield significant improvements over the AGRSST presented herein and was thus omitted for the sake of brevity. Another promising direction for future research concerns the incorporation of multiple auxiliary densities. While the optimal strategy for weighting these distinct densities to derive a final estimate remains an open question, a potential initial approach could involve formulating an overall auxiliary density as a linear convex combination of several individual auxiliary densities, with weights potentially determined through a multi-dimensional grid search aimed at maximizing $\hat{\gamma}$, the estimated correlation. However, we also note that a significantly improved (auxiliary) data situation enables more sophisticated methodologies such as random forest-based dasymetric mapping (Stevens et al., 2015). This generally raises questions regarding the relationship between AGRSST and such methods, including when one approach should be preferred over the other, and what potential combinations might be beneficial. Furthermore, future work with significant practical implications includes the extension of the Kernelheaping package to incorporate the AGRSST methodology, as well as the introduction of refinement schemes already established for the GRSST. These include the boundary correction technique and the capacity to exclude (uninhabited) areas known to have a density of zero from the estimation process (Erfurth et al. (2022)).

Overall, our research demonstrates the considerable potential that auxiliary densities offer in the context of density estimation with aggregated data. We recommend that practitioners consider using AGRSST when the emphasis is on limiting potential adverse effects from incorporating an auxiliary density, and AGRSST1 when the focus is on maximizing potential accuracy. In any case, considering the generally poor initial data situation, which largely prohibits advanced statistical modeling and uncertainty quantification techniques such as cross-validation, a sound theoretical justification for the candidate auxiliary density is indispensable.

Acknowledgements

The generative AI tools ChatGPT-4o, Gemini 2.0 Flash, and Claude 3.7 Sonnet were used to improve the language, grammar, and structure of this submission. They were also employed as search engines for research purposes. The core ideas, as well as the creative and critical thinking behind this work, are solely attributed to the authors.

Declarations

Funding and/or Conflicts of interests/Competing interests

All authors declare no conflicts of interest.

Code Availability Statement

The code used in this study is available upon request from the corresponding author.

Data Statement

The hunting bag statistics for Bremen and Lower Saxony are available in the Handbook of the German Hunting Association (DJV), whose president is Dammann-Tamke (2025), and can be purchased online. All other datasets used are freely available under their corresponding citations.

References

Aubry, P., Guillemain, M., Jensen, G. H., Sorrenti, M., & Scallan, D. (2020). Moving from intentions to actions for collecting hunting bag statistics at the European scale: Some methodological insights. *European Journal of Wildlife Research*, 66(4). <https://doi.org/10.1007/s10344-020-01400-2>

Bock, A. (2020). *Lepus europaeus* (lagomorpha: Leporidae). *Mammalian Species*, 52(997), 125–142. <https://doi.org/10.1093/mspecies/seaa010>

Brandão, F. J. S., Correia, R. M., & Paio, A. (2018). Measuring urban renewal: A dual kernel density estimation to assess the intensity of building renovation—case study in lisbon. *Urban Science*, 2(3), 91. <https://doi.org/10.3390/urbansci2030091>

Celeux, G. (1985). The SEM algorithm: A probabilistic teacher algorithm derived from the EM algorithm for the mixture problem. *Computational statistics quarterly*, 2, 73–82.

Celeux, G., Chauveau, D., & Diebolt, J. (1996). Stochastic versions of the EM algorithm: An experimental study in the mixture case. *Journal of statistical computation and simulation*, 55(4), 287–314. <https://doi.org/10.1080/00949659608811772>

Dammann-Tamke, H. (2025). *DJV handbuch 2025*. Deutscher Jagdverband. <https://www.grube.de/p/djv-handbuch-2025/P76-381-2025/>

Dempster, A. P., Laird, N. M., & Rubin, D. B. (1977). Maximum likelihood from incomplete data via the EM algorithm. *Journal of the Royal Statistical Society Series B: Statistical Methodology*, 39(1), 1–22. <https://doi.org/10.1111/j.2517-6161.1977.tb01600.x>

Destatis. (2024a). Bevölkerungszahlen in Gitterzellen. https://www.zensus2022.de/static/Zensus_Veroeffentlichungen/2022/Bevoelkerungszahlen_in_Gitterzellen.pdf

Destatis. (2024b). Personen: Bevölkerungszahl, Code: 1000A-0000. <https://ergebnisse.zensus2022.de/datenbank/1000A-0000>

Didan, K., & Barreto-Muñoz, A. (2019). *MODIS collection 6.1 (C61) vegetation index product user guide* (tech. rep.). The University of Arizona, Vegetation Index and Phenology Lab: Tucson, AZ, USA. Retrieved March 26, 2025, from https://lpdaac.usgs.gov/documents/621/MOD13_User_Guide_V61.pdf

Didan, K. (2021). MODIS/Terra Vegetation Indices 16-Day L3 Global 500m SIN Grid V061. <https://doi.org/https://dx.doi.org/10.5067/MODIS/MOD13A1.061>

Elashoff, M., & Ryan, L. (2004). An EM algorithm for estimating equations. *Journal of Computational and Graphical Statistics*, 13(1), 48–65. <https://doi.org/10.1198/1061860043092>

Elvidge, C. D., Baugh, K. E., Dietz, J. B., Bland, T., Sutton, P. C., & Kroehl, H. W. (1999). Radiance calibration of DMSP-OLS low-light imaging data of human settlements. *Remote Sensing of Environment*, 68(1), 77–88. [https://doi.org/10.1016/s0034-4257\(98\)00098-4](https://doi.org/10.1016/s0034-4257(98)00098-4)

Elvidge, C. D., Zhizhin, M., Ghosh, T., Hsu, F.-C., & Taneja, J. (2021). Annual time series of global VIIRS nighttime lights derived from monthly averages: 2012 to 2019. *Remote Sensing*, 13(922). <https://doi.org/10.3390/rs13050922>

Erfurth, K., Groß, M., Rendtel, U., & Schmid, T. (2022). Kernel density smoothing of composite spatial data on administrative area level: A case study of voting data in Berlin. *ASTA Wirtschafts- und Sozialstatistisches Archiv*, 16(1), 25–49. <https://doi.org/10.1007/s11943-021-00298-9>

Federal Agency for Cartography and Geodesy, D. (2024). Verwaltungsgebiete 1:250 000. https://sgx.geodatenzentrum.de/web_public/gdz/datenquellen/Datenquellen_vg_nuts.pdf

Gräber, R., Strauß, E., Rölfing, F., & Johanshon, S. (2024). *Wild und Jagd: Landesjagdbericht* (tech. rep.). Lower Saxony Ministry of Agriculture. https://www.ml.niedersachsen.de/download/211767/Landesjagdbericht_2023_2024.pdf

Gril, L., Steinkeper, L., Groß, M., & Rendtel, U. (2025). Kernel Heaping - Kernel Density Estimation from regional aggregates via measurement error model. *The R Journal*, 16(3), 115–133. <https://doi.org/10.32614/RJ-2024-026>

Groß, M. (2016). *Messfehlermodelle für die survey-statistik und die wirtschaftsarchäologie* [Doctoral dissertation]. <http://dx.doi.org/10.17169/refubium-13584>

Groß, M., & Fuchs, L. (2022). Kernelheaping: Kernel density estimation for heaped and rounded data. <http://dx.doi.org/10.32614/cran.package.kernelheaping>

Groß, M., Kreutzmann, A.-K., Rendtel, U., Schmid, T., & Tzavidis, N. (2020). Switching between different non-hierarchical administrative areas via simulated geo-coordinates: A case study for student residents in berlin. *Journal of Official Statistics*, 36(2), 297–314. <https://doi.org/doi:10.2478/jos-2020-0016>

Groß, M., Rendtel, U., Schmid, T., Schmon, S., & Tzavidis, N. (2016). Estimating the density of ethnic minorities and aged people in berlin: Multivariate kernel density estimation applied to sensitive georeferenced administrative data protected via measurement error. *Journal of the Royal Statistical Society Series A: Statistics in Society*, 180(1), 161–183. <https://doi.org/10.1111/rssa.12179>

Havet, P. (2002). Besoins de recherche et orientations d'action résultant de l'analyse de l'enquête sur les tableaux de chasse en France (1998–1999). *Zeitschrift für Jagdwissenschaft*, 48(S1), 222–235. <https://doi.org/10.1007/bf02192412>

Holt, D., Steel, D. G., Tranmer, M., & Wrigley, N. (1996). Aggregation and ecological effects in geographically based data. *Geographical Analysis*, 28(3), 244–261. <https://doi.org/10.1111/j.1538-4632.1996.tb00933.x>

Huete, A., Didan, K., Miura, T., Rodriguez, E., Gao, X., & Ferreira, L. (2002). Overview of the radiometric and biophysical performance of the MODIS

vegetation indices. *Remote Sensing of Environment*, 83(1), 195–213. [https://doi.org/10.1016/S0034-4257\(02\)00096-2](https://doi.org/10.1016/S0034-4257(02)00096-2)

Lin, Y.-P., Chu, H.-J., Wu, C.-F., Chang, T.-K., & Chen, C.-Y. (2010). Hotspot analysis of spatial environmental pollutants using kernel density estimation and geostatistical techniques. *International Journal of Environmental Research and Public Health*, 8(1), 75–88. <https://doi.org/10.3390/ijerph8010075>

McLachlan, G. J., & Krishnan, T. (2007). *The EM algorithm and extensions*. John Wiley & Sons. <http://dx.doi.org/10.1002/9780470191613>

Nielsen, S. F. (2000). The stochastic EM algorithm: Estimation and asymptotic results. *Bernoulli. Official Journal of the Bernoulli Society for Mathematical Statistics and Probability*, 6(3), 457. <https://doi.org/10.2307/3318671>

Parzen, E. (1962). On estimation of a probability density function and mode. *The Annals of Mathematical Statistics*, 33(3), 1065–1076. <https://doi.org/10.1214/aoms/1177704472>

Rao, J. N. K., & Molina, I. (2015). *Small area estimation* (Second edition). John Wiley & Sons, Inc. <https://doi.org/10.1002/9781118735855>

Rendtel, U., Neudecker, A., & Fuchs, L. (2021). Ein neues web-basiertes verfahren zur darstellung der corona-inzidenzen in raum und zeit. *ASzA Wirtschafts- und Sozialstatistisches Archiv*, 15(2), 93–106. <https://doi.org/10.1007/s11943-021-00288-x>

Rendtel, U., & Ruhanen, M. (2018). Die konstruktion von dienstleistungskarten mit open data am beispiel des lokalen bedarfs an kinderbetreuung in berlin. *ASzA Wirtschafts- und Sozialstatistisches Archiv*, 12(3–4), 271–284. <https://doi.org/10.1007/s11943-018-0235-y>

Rieck, T., Steffen, A., Schmid-Küpke, N., Feig, M., Wichmann, O., & Siedler, A. (2020). Impfquoten bei erwachsenen in deutschland – aktuelles aus der KV-impfsurveillance und der onlinebefragung von krankenhauspersonal OKaPII. (47), 3–26. <https://doi.org/http://dx.doi.org/10.25646/7658>

Rosenblatt, M. (1956). Remarks on some nonparametric estimates of a density function. *The Annals of Mathematical Statistics*, 27(3), 832–837. <https://doi.org/10.1214/aoms/1177728190>

Schai-Braun, S. C., Weber, D., & Hackländer, K. (2012). Spring and autumn habitat preferences of active European hares (*Lepus europaeus*) in an agricultural area with low hare density. *European Journal of Wildlife Research*, 59(3), 387–397. <https://doi.org/10.1007/s10344-012-0684-5>

Silverman, B. (2018). *Density estimation for statistics and data analysis*. Routledge. <http://dx.doi.org/10.1201/9781315140919>

Sliwinski, K., Ronnenberg, K., Jung, K., Strauß, E., & Siebert, U. (2019). Habitat requirements of the European brown hare (*Lepus europaeus* Pallas 1778)

in an intensively used agriculture region (Lower Saxony, Germany). *BMC Ecology*, 19(1). <https://doi.org/10.1186/s12898-019-0247-7>

Smith, R. K., Vaughan Jennings, N., & Harris, S. (2005). A quantitative analysis of the abundance and demography of European hares *Lepus europaeus* in relation to habitat type, intensity of agriculture and climate. *Mammal Review*, 35(1), 1–24. <https://doi.org/10.1111/j.1365-2907.2005.00057.x>

Sorichetta, A., Hornby, G. M., Stevens, F. R., Gaughan, A. E., Linard, C., & Tatem, A. J. (2015). High-resolution gridded population datasets for Latin America and the Caribbean in 2010, 2015, and 2020. *Scientific Data*, 2(1), 150045. <https://doi.org/10.1038/sdata.2015.45>

Stevens, F. R., Gaughan, A. E., Linard, C., & Tatem, A. J. (2015). Disaggregating census data for population mapping using random forests with remotely-sensed and ancillary data. *PLOS ONE*, 10(2), 1–22. <https://doi.org/10.1371/journal.pone.0107042>

Sutton, P., Roberts, D., Elvidge, C., & Baugh, K. (2001). Census from Heaven: An estimate of the global human population using night-time satellite imagery. *International Journal of Remote Sensing*, 22(16), 3061–3076. <https://doi.org/10.1080/01431160010007015>

Sutton, P. (1997). Modeling population density with night-time satellite imagery and GIS. *Computers, Environment and Urban Systems*, 21(3–4), 227–244. [https://doi.org/10.1016/s0198-9715\(97\)01005-3](https://doi.org/10.1016/s0198-9715(97)01005-3)

Wang, B., & Wang, X. (2007). Bandwidth selection for weighted kernel density estimation. *arXiv e-prints*, arXiv:0709.1616. <https://doi.org/10.48550/arXiv.0709.1616>

Wei, G. C. G., & Tanner, M. A. (1990). A monte carlo implementation of the EM algorithm and the poor man's data augmentation algorithms. *Journal of the American Statistical Association*, 85(411), 699. <https://doi.org/10.2307/2290005>

Wu, B., Yang, C., Wu, Q., Wang, C., Wu, J., & Yu, B. (2023). A building volume adjusted nighttime light index for characterizing the relationship between urban population and nighttime light intensity. *Computers, Environment and Urban Systems*, 99, 101911. <https://doi.org/10.1016/j.compenvurbsys.2022.101911>

Wu, C. F. J. (1983). On the convergence properties of the EM algorithm. *The Annals of Statistics*, 11(1). <https://doi.org/10.1214/aos/1176346060>

Yang, Z., He, S., Zhang, H., Li, M., & Liang, Y. (2022). Spatiotemporal analysis of gastrointestinal tumor (GI) with kernel density estimation (KDE) based on heterogeneous background. *International Journal of Environmental Research and Public Health*, 19(13), 7751. <https://doi.org/10.3390/ijerph19137751>